Electronic Supplementary Material (ESI) for ChemComm.

Supporting information for:

Probing post-synthetic metallation in metal-organic frameworks: Insights from X-ray crystallography

Witold M. Bloch[1], Alexandre Burgun[1], Christian J. Doonan[1*], and Christopher J. Sumby[1*]

1. School of Chemistry and Physics, Centre for Advanced Nanomaterials, The University of Adelaide, Adelaide, SA 5005, Australia.

Contents

1. Experimental

1.1. Materials and measurements

Unless otherwise stated, all chemicals were obtained from commercial sources and used as received. Acetonitrile was distilled from CaH_2 and degassed with Ar. Infrared spectra were collected on a Perkin-Elmer Spectrum 100 using a UATR sampling accessory. Thermal gravimetric analysis (TGA) was performed on a Perkin-Elmer STA-6000 instrument under a constant flow of N_2 at a temperature increase rate of 10 °C/min. Powder X-ray diffraction data were collected on a Bruker Advanced D8 diffractometer (capillary stage) using Cu Kα radiation (λ = 1.5418 Å, 40 kW/40mA). Simulated powder X-ray diffraction patterns were generated from the single crystal data using Mercury 3.0. Energy-dispersive X-ray spectroscopy (EDX) was performed on a Philips XL30 field emission scanning electron microscope. MOF **1** was prepared by a previously reported procedure.[1]

1.2. Post-synthetic reactions

General procedure

The as-synthesized MOF, **1** (25.0 mg, 0.017 mmol), was washed with DMF (3 times) and solvent-exchanged (7 times) with the appropriate solvent (DMF, DMSO, methanol, ethanol, or acetonitrile). $MnCl_2 \cdot 4H_2O$ (33 mg, 0.17 mmol, 10 equiv.) was added to the vial containing **1** and the resulting mixture was placed in an oven pre-set at the appropriate temperature for 24 h. After cooling to room temperature, the resulting material solvent was exchanged for fresh methanol (7 times). The solvent was decanted, and the wet crystals were subject to a flow of N_2 for 1 h, and then heated to 100 °C for 1 h to desolvate the sample.

$\mathbf{1\cdot[Mn(H_2O)_3Cl]Cl\cdot}\boldsymbol{x}\mathbf{EtOH}$ ($\mathbf{1\cdot[Mn]\cdot}\boldsymbol{x}\mathbf{EtOH}$)

1$\cdot[MnCl_2]\cdot x$EtOH was prepared in ethanol according to the general procedure. ν_{max}(neat, cm^{-1}): 1604 (s, C=O), 1551 (m, C=C), 1509 (m, C=C) 1405 (s), 1015 (s).

$\mathbf{1\cdot[MnCl(H_2O)_3]Cl[Mn(H_2O)_3\text{-}\mu_2Cl\text{-}MnCl_3]\cdot[MnCl(CH_3CN)_2(H_2O)_3]Cl}$ $\boldsymbol{x}\mathbf{CH_3CN}$ ($\mathbf{1\cdot[Mn]\cdot}\boldsymbol{x}\mathbf{CH_3CN}$)

1$\cdot[MnCl_2]\cdot xCH_3CN$ was prepared in acetonitrile according to the general procedure. ν_{max}(neat, cm^{-1}): 1602 (s, C=O), 1543 (m, C=C), 1508 (m, C=C) 1403 (s), 1015 (s), 951 (s).

2. Thermogravimetric analysis (TGA)

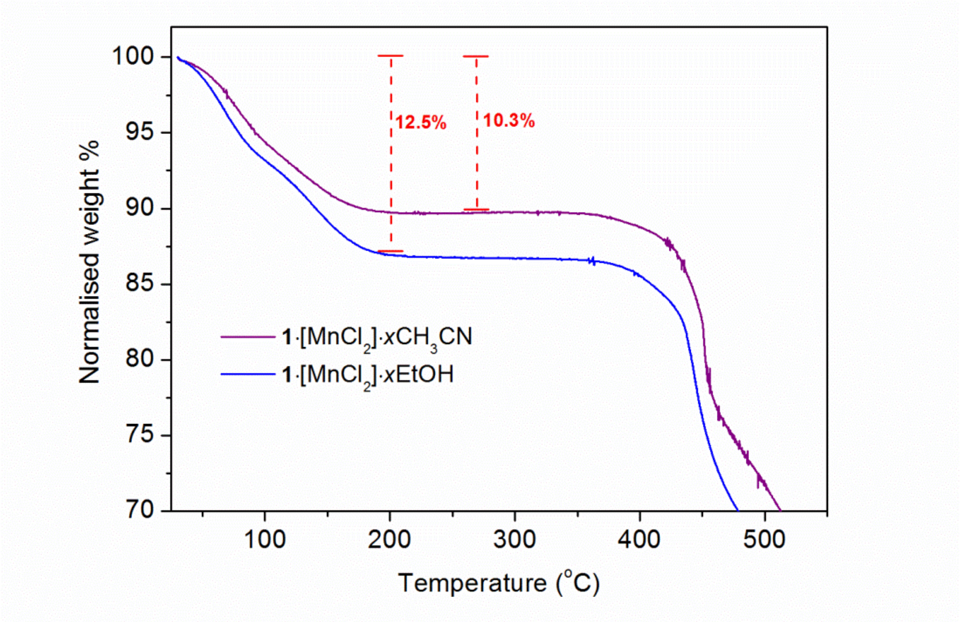

Figure SI 1. TGA traces of **1·[Mn]·*x*EtOH** and **1·[Mn]·*x*CH_3CN**. The initial weight loss of each material corresponds to loss of pore-bound solvent and the metallated MOFs are thermally stable to *ca.* 350°C.

3. Single crystal X-ray diffraction

3.1. Details of Single Crystal X-ray Diffraction Studies

Single crystals were mounted in paratone-N oil on a nylon loop. X-ray diffraction data were collected at 100(2) K on the MX-1 beamline of the Australian Synchrotron ($\lambda = 0.7107$ Å). Data sets were corrected for absorption using a multi-scan method, and structures were solved by direct methods using SHELXS-97,[2] and refined by full-matrix least squares on F^2 by SHELXL-97,[3] interfaced through the program X-Seed[4] In general, all non-hydrogen atoms were refined anisotropically and hydrogen atoms were included as invariants at geometrically estimated positions, unless specified otherwise in additional details section of the electronic supplementary information. Full details of the structure determinations have been deposited with the Cambridge Crystallographic Data Centre as CCDC #s 1037233-1037235 (specifically CCDC 1037233 - **1**·CH_3CN; CCDC 1037234 - 1·[Mn]·$x$$CH_3CN$; CCDC 1037235 - 1·[Mn]·$x$EtOH). Copies of this information may be obtained free of charge from The Director, CCDC, 12 Union Street, Cambridge CB2 1EZ, U.K. (fax, +44-1223-336-033; e-mail, deposit@ccdc.cam.ac.uk).

3.2. Selected details of data collections and structure refinements

Table SI 1. X-ray experimental data for **1**·[Mn]·*x*EtOH, **1**·[Mn]·*x*CH_3CN, and **1**·CH_3CN.

Compound	**1**·[Mn]·*x*EtOH	**1**·[Mn]·*x*CH_3CN	**1**·CH_3CN
Empirical formula	$C_{75}H_{66}N_{12}O_{15}Mn_4Cl_2$	$C_{77}H_{69}N_{13}O_{16.5}Mn_{5.5}Cl_{5.25}$	$C_{75}H_{63}N_{12}O_{12}Mn_3$
Formula weight	1666.06	1928.73	1489.19
Crystal system	Monoclinic	Monoclinic	Triclinic
Space group	*P*2_1/*m*	*P*2_1/*m*	*P*-1
a (Å)	12.355(3)	12.338(3)	12.281(3)
b (Å)	33.452(7)	33.330(7)	12.919(3)
c (Å)	12.952(3)	25.857(5)	30.425(6)
α (º)	90	90	94.65(3)
β (º)	97.63(3)	97.45(3)	93.93(3)
γ (º)	90	90	92.40(3)
Volume (Å^3)	5305.6(19)	10543(4)	4794.5(19)
Z	2	4	2
Density (calc.) (Mg/m^3)	1.043	1.215	1.032
Absorption coefficient (mm^{-1})	0.568	0.830	0.442
F(000)	1708	3923	1536
Crystal size (mm^3)	0.29×0.09×0.04	0.24×0.08×0.02	0.10×0.04×0.02
θ range for data collection (º)	1.663 to 27.284	0.794 to 31.392	1.346 to 27.918
Reflections collected	85469	200686	81010
Observed reflections [R(int)]	11393 [0.0674]	30063 [0.0722]	21017 [0.0780]
Goodness-of-fit on F^2	1.029	1.021	0.964
R_1 [$I>2\sigma(I)$]	0.0890	0.1187	0.0585
wR_2 (all data)	0.2636	0.3259	0.1563
Largest diff. peak and hole (e.Å^{-3})	1.012 and -1.940	2.191 and -3.379	0.991 and 0.957
Parameters	575	1158	934
Restraints	0	1	0

3.3. Specific details of each refinement

Structure of 1·[Mn]·*x*EtOH: The diffrn_measured_fraction_theta_full is low (94.1%). This is low due to the constraints of the goniometer (phi rotation) and the orientation of the crystal during this particular data collection. It is not possible to remove and remount crystals of this sample following a data collection at 100K (the crystals collapse upon warming) to improve completeness. Datasets with better completeness have been obtained but the quality of these individual crystals were lower and provided a less satisfactory refinement. The structure has large solvent accessible voids. These contained a number of diffuse electron density peaks that could not be adequately identified and refined as solvent. The SQUEEZE routine of PLATON was applied to the collected data, which resulted in significant reductions in R_1 and wR_2 and an improvement in the GOF. R_1, wR_2 and GOF before SQUEEZE routine: 15.02%, 43.73%, 1.822; after SQUEEZE routine: 8.90%, 26.36%, 1.029. The contents of the solvent region calculated from the result of SQUEEZE routine equates to 9 ethanol molecules.

Structure of 1·[Mn]·*x*CH_3CN: The structure also has large solvent accessible voids. Within these voids there was region of electron density which was modelled as disordered chloride and $MnCl_4^{2-}$ counter-ions based on peaks in the difference map; two chloride ions and a $MnCl_4^{2-}$ anion were assigned with 50% (each) and 50% occupancy respectively. An additional negatively charged species (-1) to provide a charge neutral framework could not be located in the difference map. Furthermore, the solvent accessible voids contained other diffuse electron density peaks that could not be adequately identified and refined as solvent. The SQUEEZE routine of PLATON was applied to the collected data, which resulted in significant reductions in R_1 and wR_2 and an improvement in the GOF. R_1, wR_2 and GOF before SQUEEZE routine: 17.35%, 51.41%, 2.242; after SQUEEZE routine: 11.89%, 32.77%, 1.020. The exact nature of the species in the solvent accessible region calculated from the result of SQUEEZE routine could not be determined due to uncertainties in the form of the additional anion (Cl^- vs $MnCl_4^{2-}$).

Structure of 1·CH_3CN: The diffrn_measured_fraction_theta_full is low (93.6%). This is low due to the constraints of the goniometer (phi rotation) and the orientation of the crystal during this particular data collection. It is not possible to remove and remount crystals of this sample following a data collection at 100K (the crystals collapse upon warming) to improve completeness. Datasets with better completeness have been obtained but the quality of these individual crystals were lower and provided a less satisfactory refinement. The structure has large solvent accessible voids. These contained a number of diffuse electron density peaks that could not be adequately identified and refined as solvent. The SQUEEZE routine of PLATON was applied to the collected data, which resulted in significant reductions in R_1 and wR_2 and an improvement in the GOF. R_1, wR_2 and GOF before SQUEEZE routine: 14.81%, 45.17%, 1.757; after SQUEEZE routine: 5.85%, 15.63%, 0.964. The contents of the solvent region calculated from the result of SQUEEZE routine equates to 11 acetonitrile molecules.

Within **1·CH_3CN** one $MnCl_4$ unit is coordinated and very well ordered/behaved (low thermal parameters). The other $MnCl_4$ unit was located during a search for counterions within pockets in the structure that normally contain anions (based on our previous published[1] and unpublished work on this MOF). This region of electron density is badly disordered but based on the appearance of a tetrahedral species with bond lengths similar to the coordinated $MnCl_4$ unit previously identified we assigned this region of electron density to a partially occupied $MnCl_4$ anion and two chloride anions. $[MnCl_4]^{2-}$ counter-ions are common in coordination complexes of manganese(II) and this species has bond lengths consistent with other examples of this anion (see the manuscript for references). Given the disorder present in this region of the structure we cautiously restricted ourselves to the assignment provided and only undertook limited refinement of these atom positions.

3.4. 50% probability thermal ellipsoids

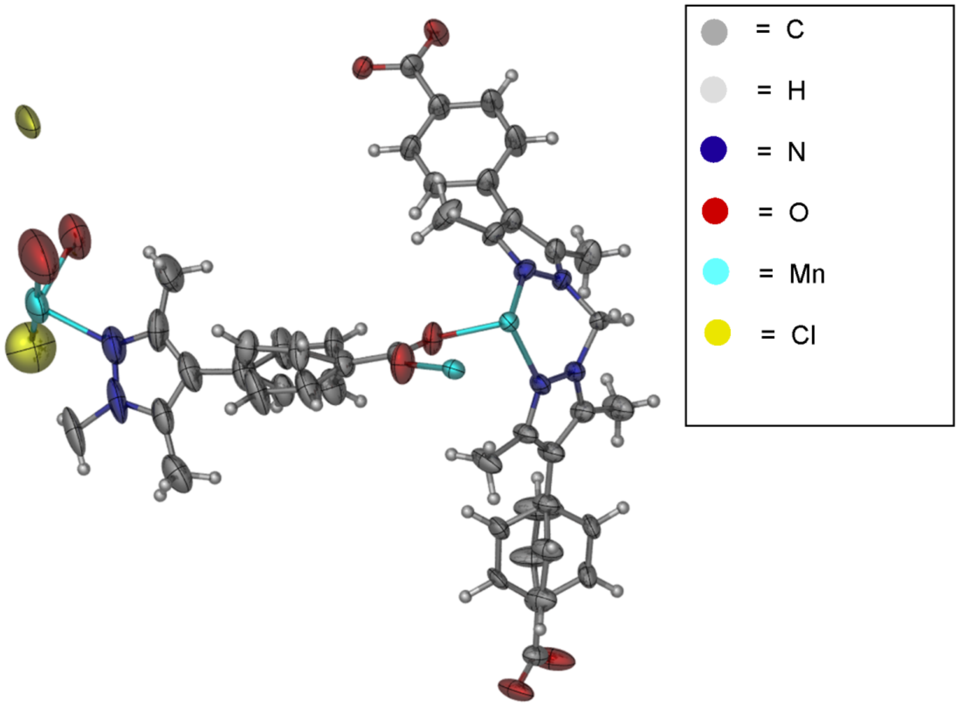

Figure SI 2. The asymmetric unit of **1**·[Mn]·xEtOH, with all non-hydrogen atoms shown as ellipsoids at the 50% probability level.

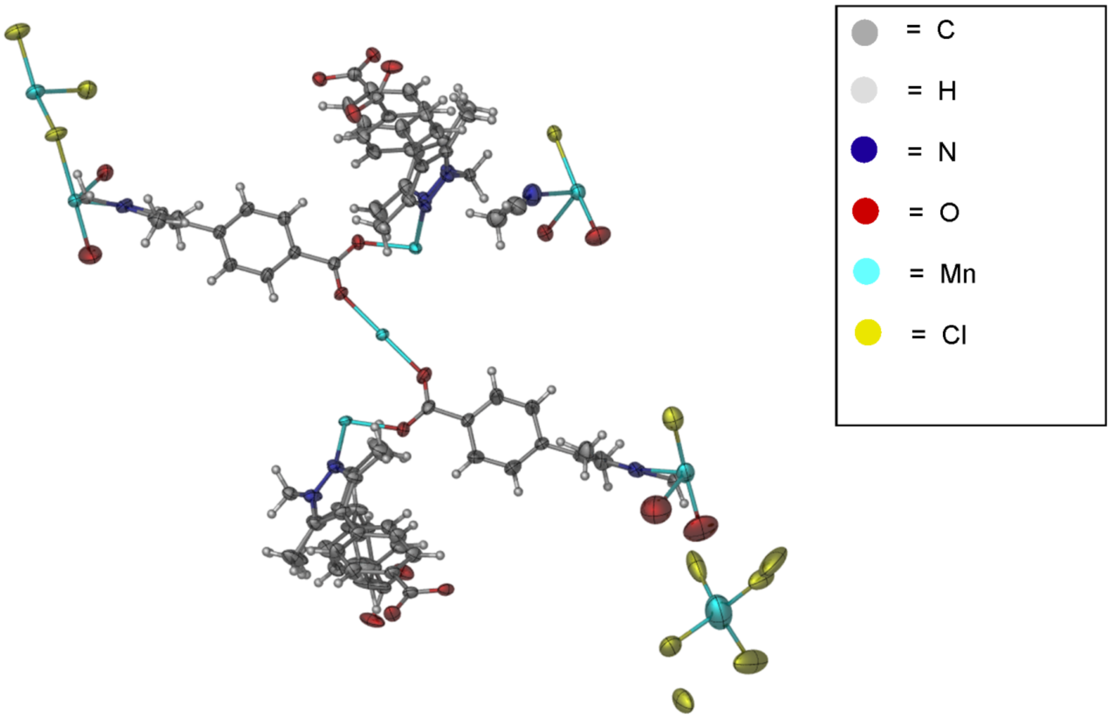

Figure SI 3. The asymmetric unit of **1**·[Mn]·$x\mathrm{CH_3CN}$, with all non-hydrogen atoms shown as ellipsoids at the 50% probability level.

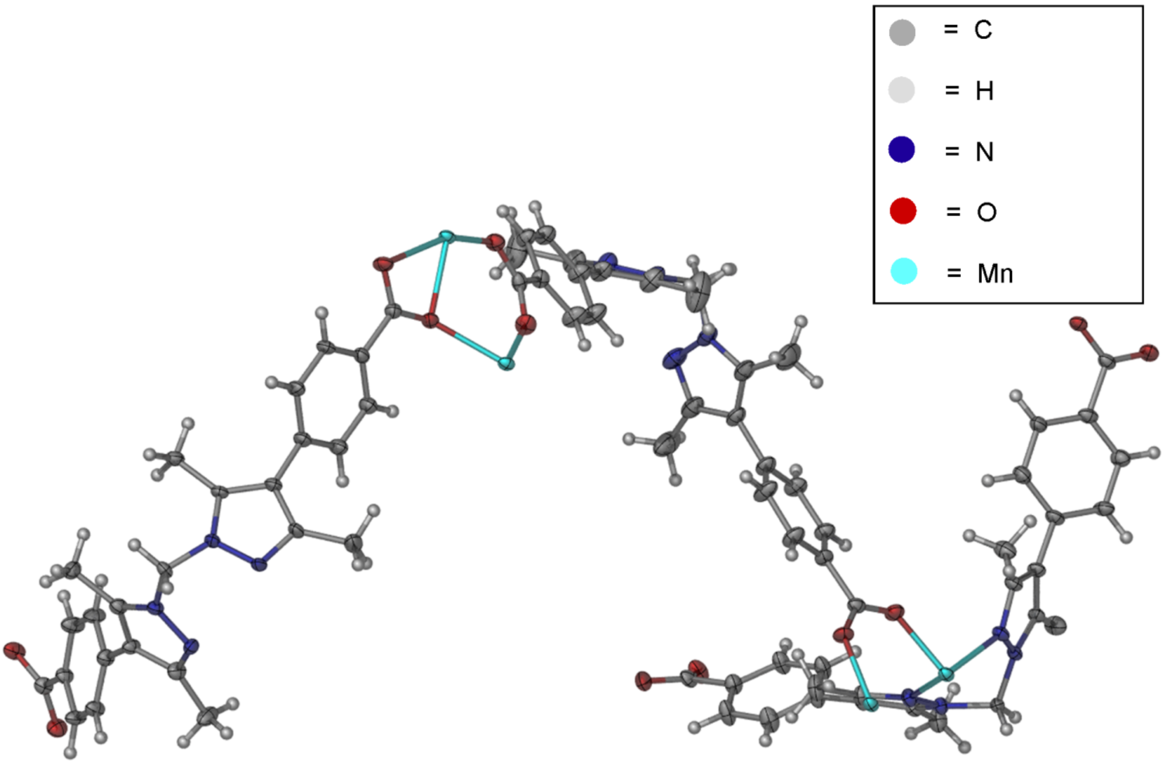

Figure SI 4. The asymmetric unit of **1**·xCH$_3$CN, with all non-hydrogen atoms shown as ellipsoids at the 50% probability level.

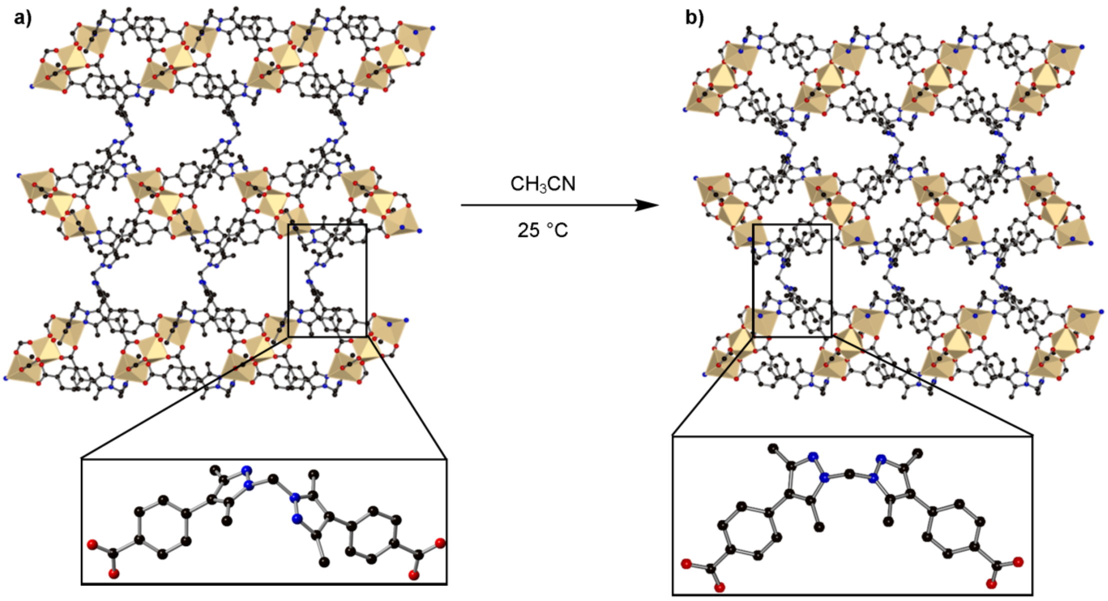

Figure SI 5. A scheme depicting the solid-state transformation that occurs when **1**·DMF (a) is solvent exchanged with CH_3CN to yield **1**·CH_3CN (b). The inset shows the rotation of the free di-pyrazole moiety within the MOF.

Table SI 2. Refined site occupancy factors of the post-synthetically inserted metal ions in **1**·[Mn]·*x*EtOH and **1**·[Mn]·*x*CH_3CN.

Structure	Atom refined	Refined Occupancy
1·[Mn]·*x*EtOH	Mn	0.795[a]
1·[Mn]·*x*CH_3CN	Mn	0.975[b]
	Mn	0.888[c]

[a] Metal ion located on a crystallographic mirror plane.

[b] Average of three atoms over two crystallographically unique sites.

[c] Manganese atom part of a isolated complex located in the pores of **1.**

4. Energy dispersive X-ray spectroscopy (EDX)

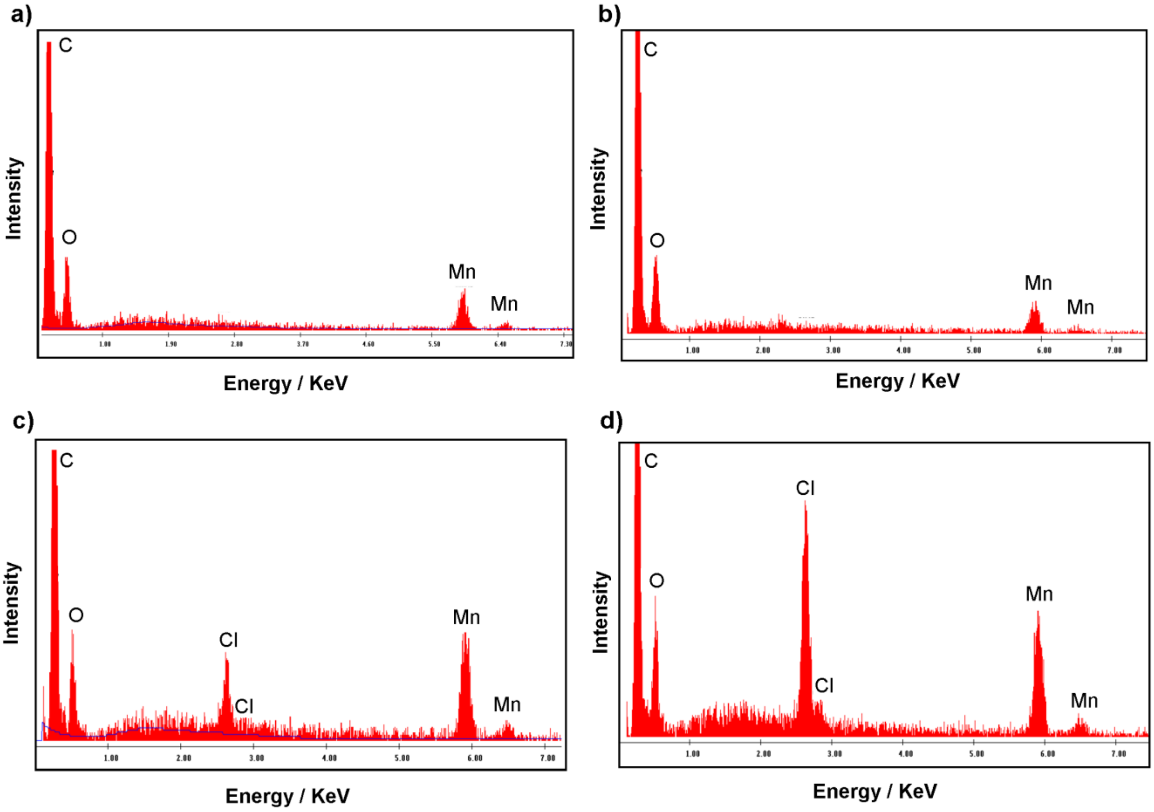

Figure SI 6. Examples of raw EDX spectra: (a) **1** synthesised with a 10-fold excess of $MnCl_2 \cdot 4H_2O$; (b) **1** treated with $MnCl_2 \cdot 4H_2O$ at 120 °C for 24 h; (c) **1** treated with $MnCl_2 \cdot 4H_2O$ at 85 °C for 24 h (**1**·[Mn]·*x*EtOH); (d) **1** treated with $MnCl_2 \cdot 4H_2O$ at 65 °C for 24 h (**1**·[Mn]·*x*CH_3CN).

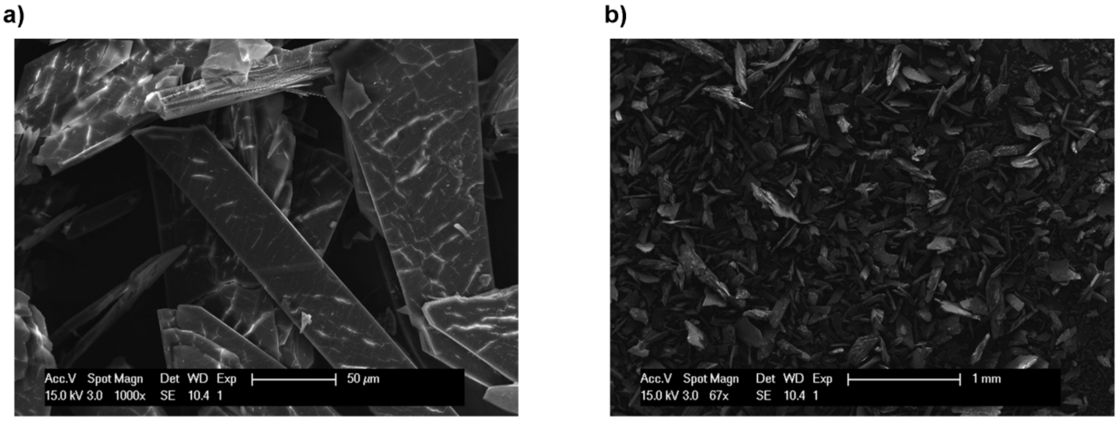

Figure SI 7. SEM images of a selected sample of **1**; (a) an example of a single crystal; (b) an example of an area of crystals used for analysis.

5. Powder X-ray diffraction (PXRD)

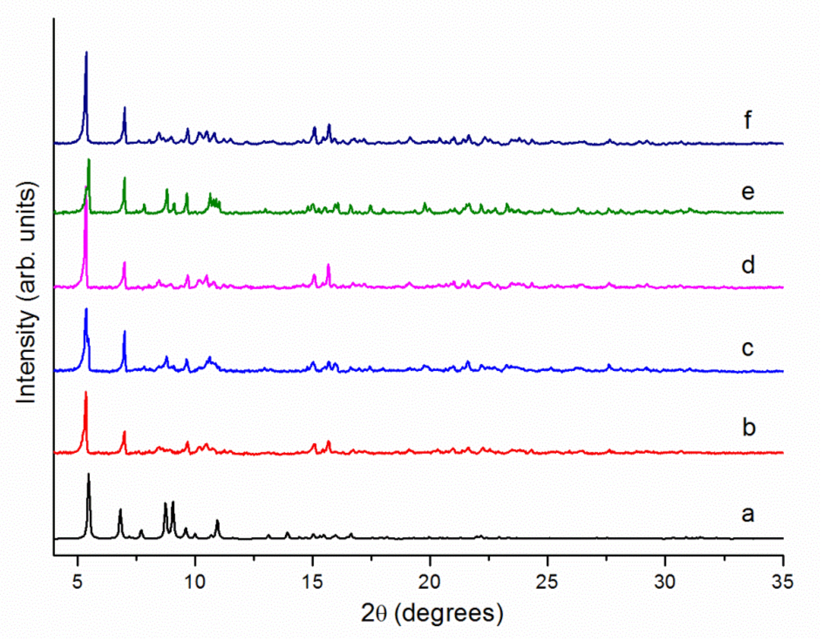

Figure SI 8. PXRD patterns of (a) **1**·DMF simulated; (b) **1** synthesised with a 10-fold excess of $MnCl_2·4H_2O$; (c) **1**·DMF treated with $MnCl_2·4H_2O$ at 65°C; (d) **1**·DMF treated with $MnCl_2·4H_2O$ at 100°C; (e) **1**·DMF treated with $MnCl_2·4H_2O$ at 120°C; and (f) **1**·DMF/H_2O treated with $MnCl_2·4H_2O$ at 100°C.

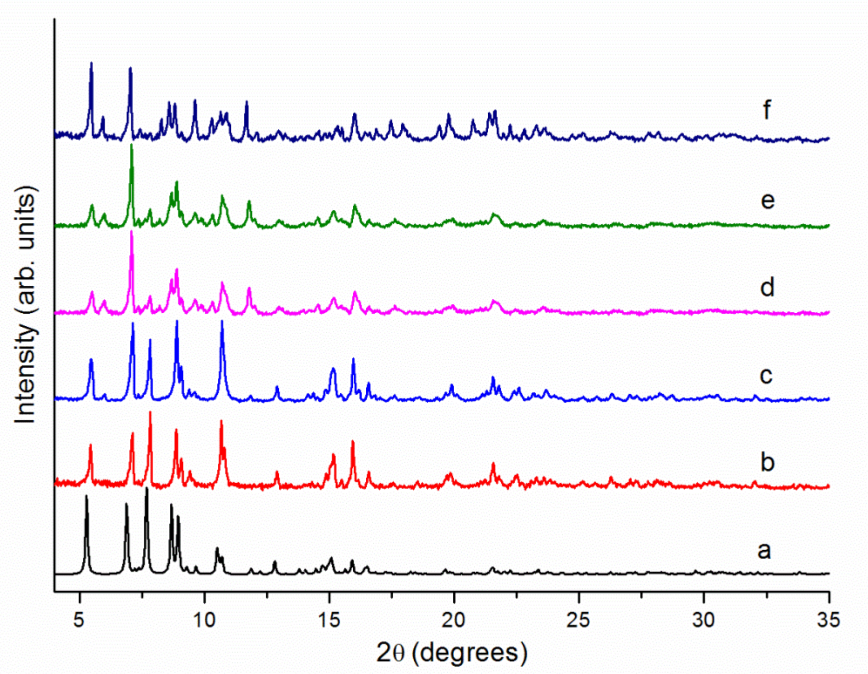

Figure SI 9. PXRD patterns of (a) **1**·[Mn]·*x*EtOH simulated; (b) **1**·EtOH treated with $MnCl_2·4H_2O$ at 65°C; (c) **1**·EtOH treated with $MnCl_2·4H_2O$ at 85°C; (d) **1**·MeOH treated with $MnCl_2·4H_2O$ at 65°C; (e) **1**·MeOH treated with $MnCl_2·4H_2O$ at 85°C; and (f) **1**·DMSO treated with $MnCl_2·4H_2O$ at 65°C.

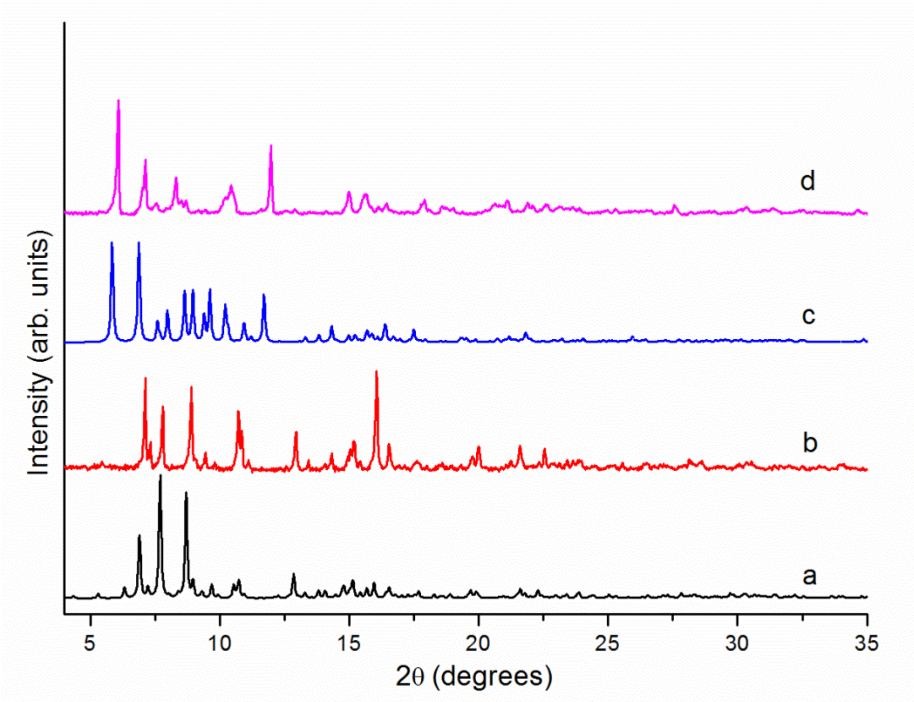

Figure SI 10. PXRD patterns of (a) **1**·[Mn]·*x*CH_3CN simulated; (b) **1**·CH_3CN treated with $MnCl_2 \cdot 4H_2O$ at 65°C; (c) **1**·CH_3CN simulated; and (d) **1**·CH_3CN treated with $MnCl_2 \cdot 4H_2O$ at 25°C.

6. Gas adsorption isotherms and pore size distributions

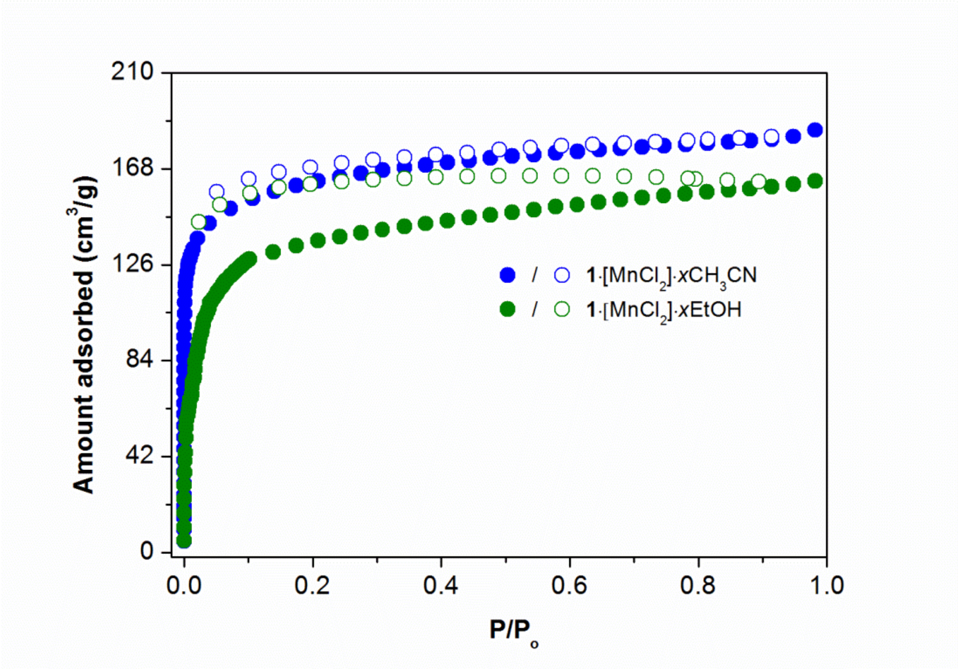

Figure SI 11. 77 K N_2 adsorption isotherm of **1**·[Mn]·*x*CH_3CN and **1**·[Mn]·*x*EtOH. An N_2 absorption hysteresis is not observed for the non-metallated MOF.[1] In the examples given here, hysteresis is likely due to the metallisation giving rise to a more complex pore structure and the desorption from this complex pore structure affording a hysteresis loop.[5]

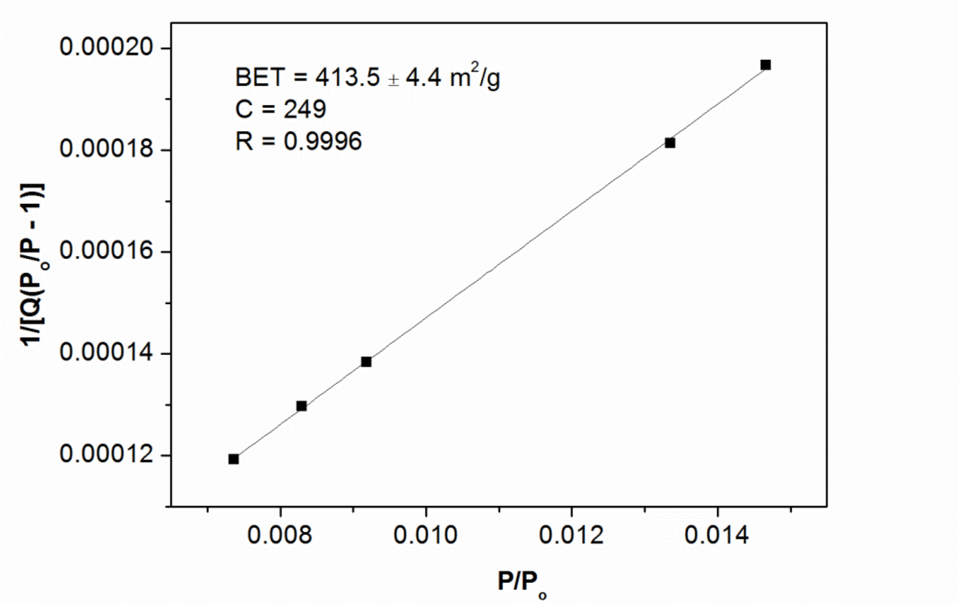

Figure SI 12. Derivation of BET surface area from the 77 K N_2 adsorption isotherm of **1**·[Mn]·*x*EtOH.

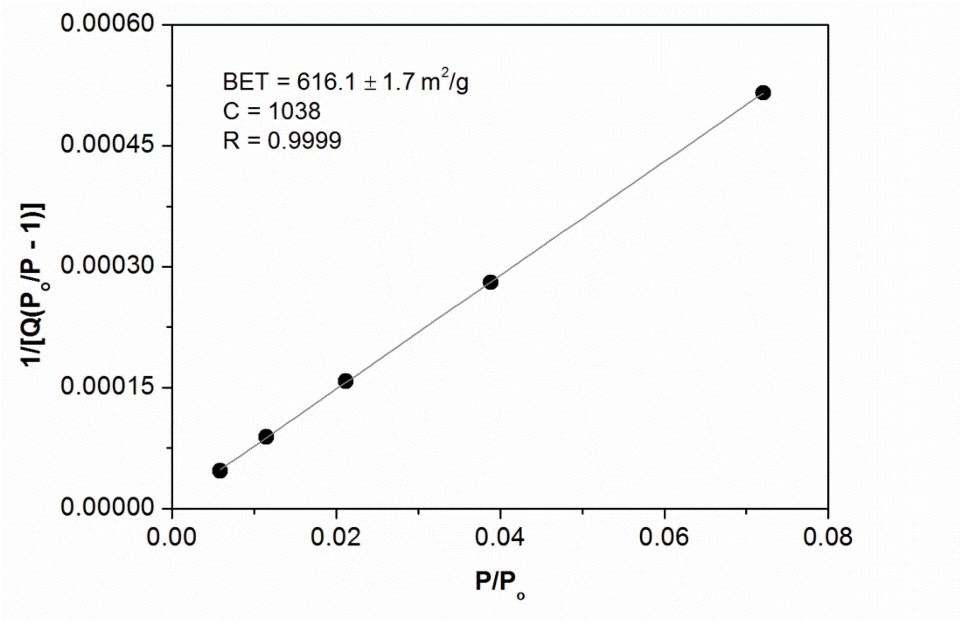

Figure SI 13. Derivation of BET surface area from the 77 K N_2 adsorption isotherm of **1**·[Mn]·*x*CH_3CN.

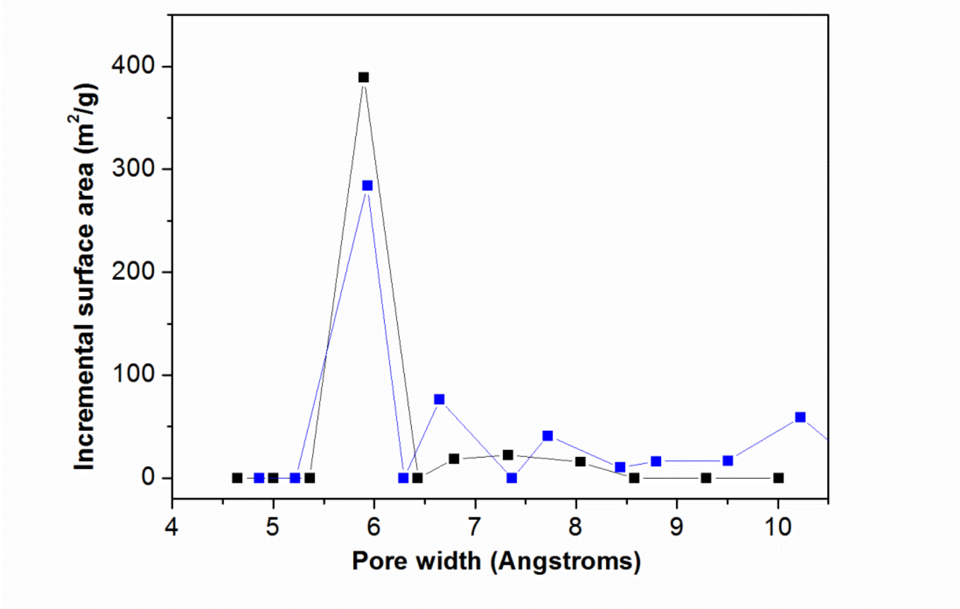

Figure SI 14. Pore size distribution obtained from the 77 K N_2 isotherm of **1**·[Mn]·*x*CH_3CN and **1**·[Mn]·*x*EtOH. The data was processed using Micromeritics ASAP 2020 software.

7. References

1. W. M. Bloch, A. Burgun, C. J. Coghlan, R. Lee, M. L. Coote, C. J. Doonan and C. J. Sumby, *Nat. Chem.*, 2014, **6**, 906-912.
2. G. M. Sheldrick, *Acta Crystallogr., Sect. A*, 1990, **46**, 467-473.
3. G. M. Sheldrick, *SHELXL-97*, University of Göttingen, Göttingen, Germany, 1997.
4. L. J. Barbour, *J. Supramol. Chem.*, 2001, **1**, 189-191.
5. Phuong T.M. Nguyen, D.D. Do, D. Nicholson, *Colloids Surf., A.*, 2013, **437**, 56-68.